Journal of Molecular Structure 1143 (2017) 265–273

Contents lists available at ScienceDirect

Journal of Molecular Structure

journal homepage: http://www.elsevier.com/locate/molstruc

Franck Condon spectra of the 2-tolunitrile dimer and the binary 2-tolunitrile water cluster in the gas phase

Felix Gmerek, Benjamin Stuhlmann, Elvedina Pehlivanovic, Michael Schmitt*

Heinrich-Heine-Universität, Institut für Physikalische Chemie I, D-40225 Düsseldorf, Germany

ARTICLE INFO

Article history:
Received 23 March 2017
Received in revised form
22 April 2017
Accepted 24 April 2017
Available online 26 April 2017

Keywords:
Franck-Condon analysis
2-Tolunitrile dimer
Water cluster
Structure
Excitonic splitting

ABSTRACT

We present fluorescence emission spectra of the 2-tolunitrile dimer and the 2-tolunitrile water cluster through various vibronic bands in the electronically excited state. From the transition dipole moments in the individual monomers, the 2-TN dimer has shown to form J-aggregates, which is why the one-photon allowed transition is the S_1 state in this cluster in contrast to other symmetric dimers, which tend to form H-aggregates. The changes of the molecular structures upon electronic excitation have been determined from a fit of the intensities in various fluorescence emission spectra. The excited state structure of the 2-TN dimer has been found to be asymmetric, in contrast to the ground state structure. Thus, emission takes place from one of the locally excited monomer moieties in the 2-tolunitrile dimer.

1. Introduction

The 2-tolunitrile (2-TN) dimer belongs to the same class of centrosymmetric homodimers, as the benzonitrile dimer [1–4], the benzoic acid dimer [5–7], the 2-cyanophenol dimer [8], the 3-cyanophenol dimer [9], the azaindole dimer [10], and the pyridone dimer [11,12]. The question arises, if the electronic excitation in theses homodimers is localized in one of the two equivalent chromophores or if it is delocalized over both chromophores. In a recent comprehensive study, Ottiger et al. [13] investigated the exciton (Davydov) splitting in these dimers both experimentally, as well as theoretically using a quenching model that reduces the calculated electronic exciton splitting by a factor which they showed to be the product of excited-state vibrational displacements in the monomer. Clearly, their results point to a delocalized excitation with weak to intermediate coupling. Kopec et al. [14] recently showed that the quenched excitonic splitting can be interpreted as nonadiabatic tunneling splitting related to a lower adiabatic double-minimum potential energy surface (PES), but nonadiabatically coupled to the higher PES. One of the delocalized and symmetry-adapted adiabatically split levels in the double-minimum PES has the symmetry of the S_1 state, the other of the S_2-state. It has to be noted, that the aforementioned dimers form H-aggregates [15] with nearly parallel (or antiparallel) transition dipole moment orientations. However, recently a symmetric homodimer, which forms J-aggregates [16] in a molecular beam, the m-cyanophenol dimer, has been investigated [17].

Also covalently bound bichromophoric systems show excitonic splitting, with the possibility that depending on the symmetry of the system, both S_1 and S_2 components are bright states. Zwier, Plusquellic, and co-workers have shown, that for the bichromophore diphenylmethane both the S_1 and S_2 states can be observed and that the S_1 origin can be viewed as a completely delocalized, antisymmetric combination of the zero-order locally excited states of the toluene-like chromophores [18].

Exciton splitting in symmetric dimers has been discussed starting in the late 50's and early 60's [19–22]. While the concept of excitons was originally introduced by Frenkel in order to describe the excitation of atoms in a lattice of an insulator [23], interest had rapidly been shifted to molecular excitons. Apart from the electronic exciton splitting, electronic excitation in symmetric dimers has an additional aspect, namely stabilization of the excited state through solvation. Consider electronic excitation of a monomer, which is solvated after excitation by a second (identical) monomer. If the stabilization of the monomer excited state by solvation is large enough the excitation will remain at the initially excited center.

$S_1 \leftarrow S_0$ fluorescence excitation spectra and $S_0 \leftarrow S_1$ fluorescence emission spectra of 2-, 3, and 4-tolunitrile were reported by Fujii

* Corresponding author.
E-mail address: mschmitt@uni-duesseldorf.de (M. Schmitt).

http://dx.doi.org/10.1016/j.molstruc.2017.04.092
0022-2860/

et al. [24] They determined the torsional barriers of ground and lowest excited singlet states from the low frequency torsional bands in the S_0 and the S_1 states, respectively. The ground state internal rotational parameters of 2-TN have been determined from microwave spectroscopy in the frequency ranges of 22.0–26.0 GHz and 32.0–37.0 GHz [25] and from millimeter wave spectroscopy in the frequency range 50.0–75.0 GHz [26]. Nakai and Kawai studied the torsional potential of various substituted toluenes, among them 2- and 3-tolunitrile (3-TN) [27]. They showed how a $\pi^*\sigma^*$ hyperconjugation mechanism can be used to explain their different barriers in different electronic states. Later Park et al. measured the vibronic emission spectra of the jet-cooled 2-tolunitrile [28] and 3-tolunitrile [29] in a corona-excited supersonic expansion. From a density functional theory (DFT) based analysis of the spectrum, several vibrational modes were assigned in the emission spectrum. The cationic ground state D_0 has been studied using pulsed field ionization–ZEKE photoelectron spectroscopy by Suzuki et al. [30].

Recently, Gmerek et al. [31] and Ruiz-Santoyo et al. [32] performed a combination of rotationally resolved electronic spectroscopy and Franck-Condon fits of the fluorescence emission spectra of 2- and 3-TN monomers and determined the change of the geometry upon electronic excitation *via* a Franck-Condon fit.

The 1:1 water cluster of 2-TN resembles closely the binary benzonitrile-water cluster, which has been studied by Helm et al. [33] using a combination of high resolution ultraviolet (UV) and microwave (MW) spectroscopy and Melandri et al. [34] using microwave spectroscopy. It forms a double hydrogen bond between one H-atom of the water moiety and the cyano group and the *ortho* hydrogen atom at the aromatic ring and the water O-atom.

In the present paper we will elucidate the change of the molecular structure of both complexes upon electronic excitation from a fit of the FC spectra and shed light on the question, if the excitation in the symmetric homodimer is localized or delocalized.

2. Experimental and computational details

2.1. Experiment

The experimental setup for the dispersed fluorescence (DF) spectroscopy has been described in detail elsewhere [35,36]. In short, 2-tolunitrile was evaporated at 293 K and co-expanded through a pulsed nozzle (kept at 303 K to avoid condensation) with a 500 μm orifice (General Valve) into the vacuum chamber using helium as carrier gas. The output of a Nd:YAG (SpectraPhysics INDI) pumped dye laser (Lambda-Physik, FL3002) was frequency doubled and crossed at right angles with the molecular beam. The resulting fluorescence was imaged on the entrance slit of a monochromator (Jobin Yvon, f = 1 m). The dispersed fluorescence spectrum was recorded using a gated image intensified UV sensitive CCD camera (Flamestar II, LaVision). The relative intensities were afterwards normalized to the strongest band in the spectrum, not including the resonance fluorescence band, which also contains the stray light and is therefore excluded from the FC analysis.

2.2. Ab initio calculations

Structure optimizations were performed employing Dunning's correlation consistent polarized valence triple zeta basis set (cc-pVTZ) from the Turbomole library [37,38]. The equilibrium geometries of the electronic ground and the lowest excited singlet states were optimized using the approximate coupled cluster singles and doubles model (CC2) employing the resolution-of-the-identity approximation (RI) [39–41]. The Hessians and harmonic vibrational frequencies for both electronic states, which are utilized in the FC fit and needed for calculation of the zero-point energy (ZPE), have been obtained from numerical second derivatives using the NumForce script [42] implemented in the Turbomole program suite [43]. For the cluster stabilization energies, the basis set superposition errors (BSSE) have been accounted for, using the counterpoise corrections described by Boys and Bernardi [44] and implemented in the JOBBSSE jobscript of turbomole. A natural population analysis (NBO) [45] has been performed at the CC2 optimized geometries using the wavefunctions from the CC2 calculations as implemented in the Turbomole package [43].

2.3. Franck-Condon fits

The change of a molecular geometry upon electronic excitation can be determined from a fit of the intensities of absorption or emission bands using the FC principle. According to this principle, the relative intensities of the vibronic bands depend on the overlap integrals of the vibrational wave functions of both electronic states.

The fit has been performed using the program FCFit, which has been developed in our group and described in detail before [46,47]. The program computes the FC integrals of multidimensional, harmonic oscillators mainly based on the recursion formula given in the papers of Doktorov, Malkin, and Man'ko [48,49]. and fits the geometry (in linear combinations of selected normal modes) to the experimentally determined intensities. This is simultaneously done for all emission spectra, which are obtained *via* pumping through different S_1 vibronic modes.

The FC factors of the 2-TN monomer [31] are used for calculation of the quenching factor Γ for the excitonic splitting of the dimer. This quenching factor is given by [13].

$$\Gamma = exp\left(\sum_i \frac{FCF\left(i_0^1\right)}{FCF\left(0_0^0\right)}\right) \quad (1)$$

where the sum runs over the i modes of the monomers. The summands are also referred to as Huang-Rhys factors. The vibronic splitting Δ_{vibron} is calculated from the pure electronic splitting $2V_{AB}$ using the relation [13].

$$\Delta_{vibron} = 2V_{AB}\Gamma \quad (2)$$

3. Results

3.1. Ab initio calculations

3.1.1. Structure, stabilization and vibrations

The structures of the 2-TN dimer (Fig. 1a) and the 2-TN-H_2 O water cluster (Fig. 1b) have been optimized at the CC2/cc-pVTZ level of theory in the electronic ground state and the lowest two excited singlet states, cf. Table 1. The Cartesian coordinates of both clusters in their S_0 and S_1 states are given in the online supporting material. $(2\text{-TN})_2$ is found to be a planar molecule in the electronic ground state of C_{2h} symmetry.

Its 90 vibrations transform like $\Gamma_{ired} = 30a_g + 15b_g + 16a_u + 29b_u$. Upon electronic excitation the ring geometries change differently, and the molecular symmetry of the dimer reduces to C_s. The 90 vibrations in C_s transform like 59a' + 31a", with the correlation of a_g and b_u modes in C_{2h} to a' in the C_s point group. A table with the calculated vibrational ground state frequencies, their symmetries, correlations with the excited state vibrations and largest elements of the Duschinsky matrix is found in the online supporting material (Table S6). The stabilization energy of the dimer in the electronic ground state, including ZPE and BSSE

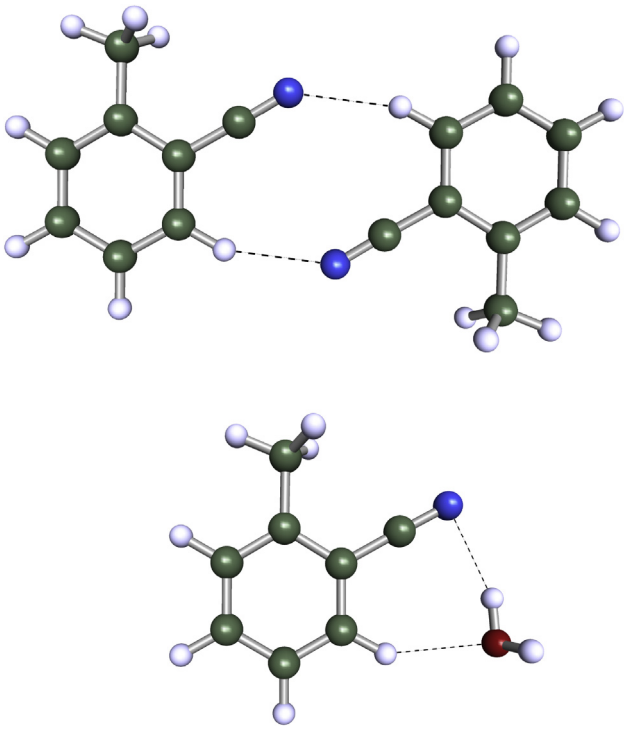

Fig. 1. Structures of $(2\text{-TN})_2$ and 2-TN-H_2 O from the optimized CC2/cc-pVTZ geometries.

Table 1
Rotational constants *A*, *B*, and *C* are given in MHz, components of the dipole moments μ_a, μ_b, and μ_c in Debye, the angle of the transition dipole moment with the a-axis θ in degrees, the angle of the transition dipole moment with the c-axis ϕ in degrees and the adiabatic excitation energies ($\nu_0^{adiab.}$) in cm^{-1}. The last four rows give the leading contributions to the transition.

	$(2\text{-TN})_2$			2-TN-H_2O	
	S_0	S_1	S_2	S_0	S_1
A	1002	988	977	1846	1827
B	163	164	161	973	959
C	141	141	139	641	633
μ_a	0.0	0.70	0.0	3.35	4.05
μ_b	0.0	0.02	0.0	0.66	0.66
μ_c	0.0	0.00	0.0	1.18	1.15
$\lvert\mu\rvert$	0.0	0.72	0.0	3.61	4.26
θ	–	−7.0	–	−11.2	−9.2
ϕ	–	90.0	–	70.9	74.3
$\nu_0^{adiab.}$	–	37377	38152	–	37.436
H → L	–	−0.75	–	–	0.76
H-2 → L+2	–	0.42	–	–	–
H-1 → L+1	–	–	–	–	0.43
H-2 → L+1	–	–	0.32	–	–
H-2 → L	–	0.34	–	–	–
H-1 → L	–	–	−0.50	–	−0.35
H → L+2	–	0.27	–	–	–
H → L+1	–	–	−0.47	–	0.27

corrections amounts to 24.1 kJ/mol, and to 26.3 kJ/mol in the lowest electronically excited state. The energetically following state has a lower stabilization energy of 20.3 kJ/mol.

Fig. 1b and Tables S4 and S5 of the online supporting material present the structure of 2-TN-H_2O. The cluster belongs to the point group C_1 in both electronic states. As in the benzonitrile-water cluster, the N-atom of the nitrile group acts as proton acceptor towards the water molecule, and the *ortho*-hydrogen atom of the aromatic ring as proton donor, leading to a cyclic structure with one hydrogen atom of the water moiety pointing out of the plane. The stabilization energy of the water cluster in the electronic ground state, including ZPE and BSSE corrections amounts to 11.5 kJ/mol, and to 13.5 kJ/mol in the electronically excited state.

3.1.2. Excitonic splitting of the 2-TN dimer

In case of a delocalized excitation the electronic origin consists of a one-photon allowed component ($^1B_u \leftarrow {}^1A_g$) and one higher (one-photon forbidden) component ($^1A_g \leftarrow {}^1A_g$). The lower B_u and the upper A_g components emerge from two locally excited harmonic oscillators with one monomer electronically excited and the other in the ground state and *vice versa*, see Fig. 2.

We calculated the vertically lowest three excited states in each symmetry of the ground state at CC2 (SCS-CC2) level of theory and found the lowest electronically excited state retaining B_u symmetry (C_{2h}) at 40111 (39258) cm^{-1} and the energetically following of A_g symmetry at 40123 (39264) cm^{-1}. Thus, the vertical excitonic splitting for the lowest electronically excited state amounts to 12 (6) cm^{-1}. The findings for the other excited states are compiled in Table 3 along vertical excitation energies, and the Cartesian components of the oscillator strengths. The exciton splitting between A_g and B_u states increases for the higher electronic states (105 (118) cm^{-1} for the splitting between S_3 and S_4 and 521 (216) cm^{-1} for the splitting between S_5 and S_6). All higher-lying electronically excited states of B_g symmetry are one-photon forbidden, and those of A_u symmetry are very weak and z-polarized (out-of-plane).

As described before the pure electronic Davydov splitting $\Delta_{el} = 2V_{AB}$ is an upper limit to the vibronic splitting Δ_{vibron}. The quenching factor Γ (see equation (1)), which accounts for the vibronic contribution, has been calculated from the FC factors, that had been determined from the FC analysis of the 2-TN monomer, given in Ref. [31] to be 0.51. Thus, the pure SCS-CC2/cc-pVTZ calculated electronic splitting is reduced to 3 cm^{-1}.

Another approach to the size of the excitonic splitting uses Frenkel exciton theory of two dipoles $\overrightarrow{\mu_1}$ and $\overrightarrow{\mu_2}$ at a distance R [11,20]. The interaction of the two dipoles is given by the dipole - dipole interaction energy V_{dd}:

$$V_{dd} = \frac{\overrightarrow{\mu_1} \cdot \overrightarrow{\mu_2}}{4\pi\varepsilon_0 R^3} \cdot \left(2(cos\theta)^2 - (sin\theta)^2 cos(\phi)\right) \quad (3)$$

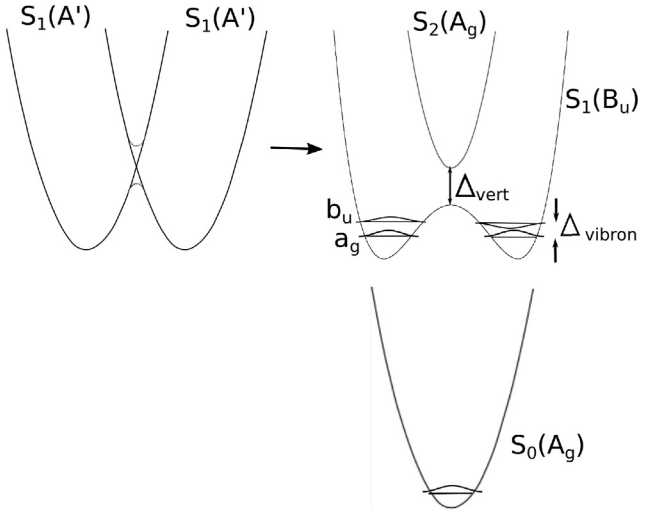

Fig. 2. Schematic drawing of the adiabatic potential energy curves of the lowest three singlet states. The left diagram shows the diabatic (S_1) states of local excitation of one of the individual monomers. On the right side, the adiabatic (delocalized) S_1 and S_2 states, emerging from the avoided crossing between the diabatic states.

The center of mass (COM) distance R of the two monomer moieties can be calculated from the inertial parameters of the dimer (I_g^{Dimer}) and the monomer ($I_g^{Monomer}$) moieties:

$$R = \sqrt{\frac{\sum_g I_g^{Dimer} - 2\sum_g I_g^{Monomer}}{M}} \tag{4}$$

where M is the mass of one monomer moiety, and the I_g are the respective moments of inertia, described by their superscripts, which are calculated from the SCS-CC2/cc-pVTZ calculated rotational constants. For reason of symmetry, the two dipole moments are equal as well as the angle θ between the dipole moments and the line connecting the two COM. The angle ϕ describes the dihedral angle between the planes containing the dipole moment vectors. Using the *ab initio* SCS-CC2/cc-pVTZ calculated values of $1.654 \cdot 10^{-30}$ Cm for the transitions dipole $\vec{\mu}$, $6.627 \cdot 10^{-10}$ m for the COM distance R, 90 ° for θ and 0 ° for ϕ one obtains a values of ±4 cm^{-1} for V_{dd} and an excitonic splitting of 8 cm^{-1}. For a more detailed discussion of the role of the angle θ for the energetic ordering see section 4.

A third approach to the vibronic splitting utilizes the Wentzel-Kramers-Brillouin (WKB) approximation [50]. The vibronic splitting, arising from the semiclassical tunneling through a barrier can be described by [51].

$$\Delta_{vibron} = \frac{\hbar\omega_f}{\pi} e^{-\theta} \tag{5}$$

where ω_f is the classical vibrational frequency in one of the wells that describes the reaction path over the barrier and θ is the barrier penetration integral, which is calculated according to:

$$\theta = \frac{2\pi}{\hbar\omega_i}\left(V_{eff} - \sqrt{E_0 V_{eff}}\right) \tag{6}$$

Here, ω_i is the imaginary frequency, which describes the motion that leads over the top of the barrier, V_{eff} is the effective barrier height and E_0 the zero-point energy of the vibration ω_f. The effective barrier height is obtained from the vibrational frequencies in the potential well ω_k and at the top of the barrier ω_k^*:

$$V_{eff} = V_0 + \sum_{k=1}^{F-1} \frac{1}{2}\left(\hbar\omega_k^* - \hbar\omega_k\right) \tag{7}$$

For small electronic Davydov splittings Δ_{vert}, the barrier height V_0 can be approximated by the difference of the adiabatic excitation energies of S_1 and S_2 state, respectively (cf. Fig. 2). The imaginary barrier penetrating vibration ω_i and the vibration in the well, which describes the reaction coordinate are excluded from the summation in equation (7). The sum in equation (7) gives the adiabatic contribution of the remaining $F - 1$ vibrational degrees of freedom to the one-dimensional tunneling motion.

Using the results of normal mode calculations of the S_1 at the minimum structure and at the transition state one obtains for the sum in equation (7) a value of 956 cm^{-1}. The value of V_0 is given by the difference of the adiabatic excitation energies of S_1 and S_2 state and amounts to 775 cm^{-1}. With a reaction coordinate wavenumber of 1067 cm^{-1} and an imaginary vibration of 1022 cm^{-1} one obtains a splitting Δ_{vibron} of 3.0 cm^{-1} in very good agreement with the values obtained from Frenkel theory and from the reduced Davydov splitting.

3.1.3. Adiabatic excitation of the 2-TN dimer

The zero-point energy corrected adiabatic excitation energy for the $S_1 \leftarrow S_0$ transition to the lowest excited state has been computed at the SCS-CC2/cc-pVTZ level of theory and amounts to 37377 cm^{-1}. Adiabatic excitation leads to an excited state, with a reduced symmetry of C_s. The locally electronically excited state, therefore has a permanent dipole moment of $2.4 \cdot 10^{-30}$ Cm (0.72 Debye) compared to the electronic ground state, which for its inversion symmetry has a zero dipole moment. Rotational constants and permanent dipole moment components of this (locally excited) state are compiled in Table 1.

The excitation to the lowest excited singlet state in C_s symmetry is composed of −0.75 (HOMO → LUMO) + 0.27 (HOMO → LUMO+2) + 0.34 (HOMO-2 → LUMO) + 0.42 (HOMO-2 → LUMO+2). The respective frontier orbitals are depicted in Fig. 3, along with the orbitals of the 2-TN-water cluster for comparison. Notably, in the lower excited state of the dimer only orbitals are connected, which have non-zero coefficients in the same (excited) monomer moiety.

The adiabatically following state was optimized without symmetry constraints, but has converged to a C_{2h} symmetric structure, like the S_0 state. Like the S_0 it is of A_g-symmetry and has consequently no permanent dipole moment, cf. Table 1. The geometry optimization of this state has been performed starting from the optimized S_0 structure as well as from the optimized S_1 structure. Both optimizations converged to a C_{2h} symmetric state for the S_2.

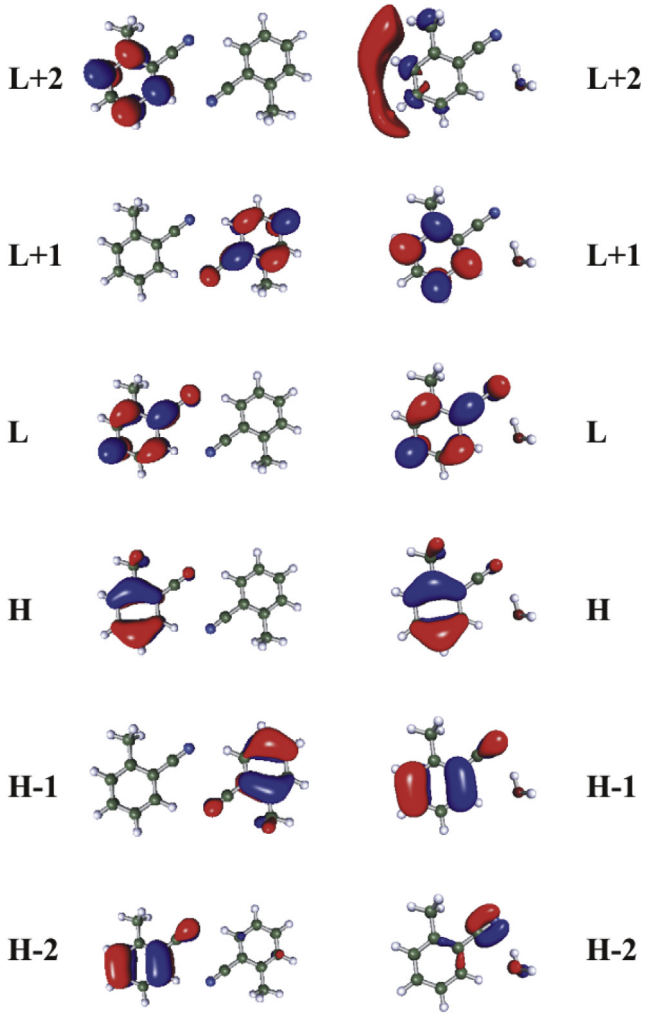

Fig. 3. Frontier orbitals of $(2\text{-TN})_2$ and 2-TN-H_2 O from the optimized CC2/cc-pVTZ geometries.

This excited state connects exclusively orbitals with non-zero coefficients in different monomer moieties, making this transition forbidden: 0.32 (HOMO-2 → LUMO+1) - 0.50 (HOMO-1 → LUMO) - 0.50 (HOMO → LUMO+1).

The converged S_2 state structure is a true minimum as proven by a normal mode analysis. The vibrational frequencies of the S_2 state are given in the online supporting material. One vibration is found to be very remarkable in the sense, that its wavenumber and its intensity are much higher than expected for a "normal" vibration. Indeed, this vibration is an artifact, due to the fact that the S_1 and the S_2-states are quasi-degenerate. Inspection of the distortion vectors of this vibration shows, that one of the aromatic rings increases, while the other decreases, thus representing the transition state coordinate which interconnects the two S_1 minima (cf. Fig. 2). At the S_2 state minimum S_2 and S_1 are quasi-degenerate and the distortion along this coordinate flips the electronically excited states, causing on one hand side a very steep potential, which leads to the high frequency and secondly a huge change of the dipole moment, which is the reason for the enormous intensity (see Fig. 2).

The rotational constants of the S_1 and S_2 states are shown in Table 1. The structure at the minimum of S_2 PES has the bond length changes symmetrically distributed over both monomers, while the bond length changes at either of the S_1 minima are localized at one of the monomers. The changes of the bond lengths upon electronic excitation from the ground state are compared in Fig. 4.

In the S_1 state one monomer remains nearly completely in the S_0 state geometry, while the changes of the other monomer moiety upon excitation to the S_1 are close to those of the monomer. Thus, the electronically excited 2-TN monomer is solvated by the second moiety in its lowest excited singlet state. Only very small changes occur, due to inductive effects. Both hydrogen bonds change very asymmetrically. For the excited moiety, in which the CN group is the proton acceptor, the bond length decreases by 5.0 pm, while the other CN···H bond decreases by 2.8 pm.

In the S_2 state all bond length changes in the two monomer moieties are identical, thus the inversion symmetry of the ground state is retained. Both hydrogen bonds increase symmetrically by 8.1 pm. This increase is reflected in the decrease of binding energy

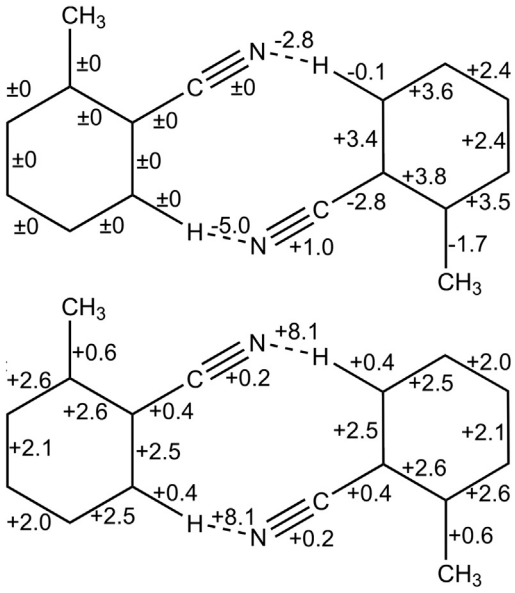

Fig. 4. Changes of the bond lengths of the 2-TN dimer upon excitation to the S_1 (upper structure) and the S_2 state (lower structure), respectively.

Table 2
CC2/cc-pVTZ calculated stabilization energies in kJ/mol of the 2-TN dimer and the 2-TN-H_2 O cluster, respectively. Stabilization energies contain zero-point energy and correction of the counter-poise computed BSSE, with the exception of the S_2 state.

	$(2\text{-TN})_2$	2-TN-H_2O
S_0	24.1	11.5
S_1	26.3	13.5
S_2	20.3	–

Table 3
Electronically excited states of C_{2h} symmetric $(2\text{-TN})_2$. The vertical excitation energy $\nu_{vert.}$ is given in cm^{-1}.

State	Sym.	CC2	SCS-CC2	f_x	f_y	f_z
1	B_u	40111	39258	0.2	0.1	0.0
2	A_g	40123	39264	0.0	0.0	0.0
3	A_g	47943	48052	0.0	0.0	0.0
4	B_u	48048	48170	3.3	0.4	0.0
5	A_g	55153	56319	0.0	0.0	0.0
6	B_u	55674	56535	2.7	3.0	0.0

of the cluster in the S_2 state, compared to the binding energy in the S_0 state, cf. Table 2, while the increase in the S_1 state shows up in a reduction of the intermolecular bond lengths.

3.2. Experimental results

3.2.1. Fluorescence excitation spectra of $(2\text{-TN})_2$ and 2-TN-H_2O

Fig. 5 shows the fluorescence excitation spectrum of 2-TN entrained into an helium molecular beam, which is recorded to the red of the monomer origin. Several bands appear in the region of 200 cm^{-1} to the red of the monomer origin, which show a distinct intensity variation upon variation of the helium backing pressure.

An additional band at about 100 cm^{-1} to the red of the monomer origin increased, with increasing partial pressure of water vapor, which is seeded into the molecular beam and co-expanded with 2-TN. Therefore, we assigned the band system starting at −209 cm^{-1} to the red of the monomer as belonging to the 2-TN dimer, and the band at 96 cm^{-1} to the red of the origin of the monomer as 1:1 water cluster of 2-TN. The water cluster of benzonitrile is found to be 70 cm^{-1} red-shifted from the benzonitrile

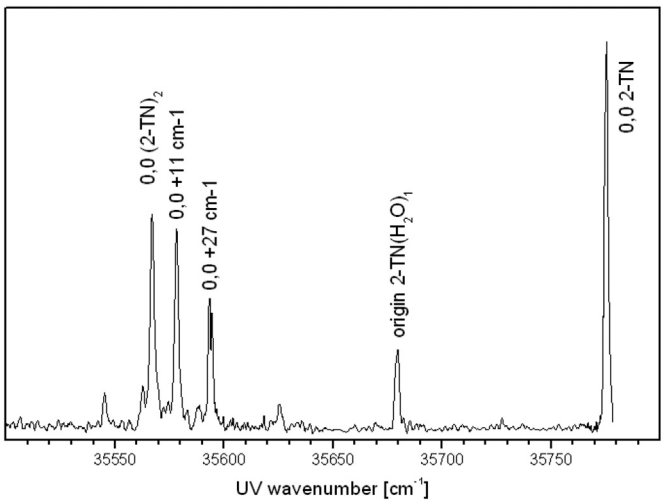

Fig. 5. Fluorescence excitation spectrum of 2-TN, $(2\text{-TN})_2$ and 2-TN-H_2O.

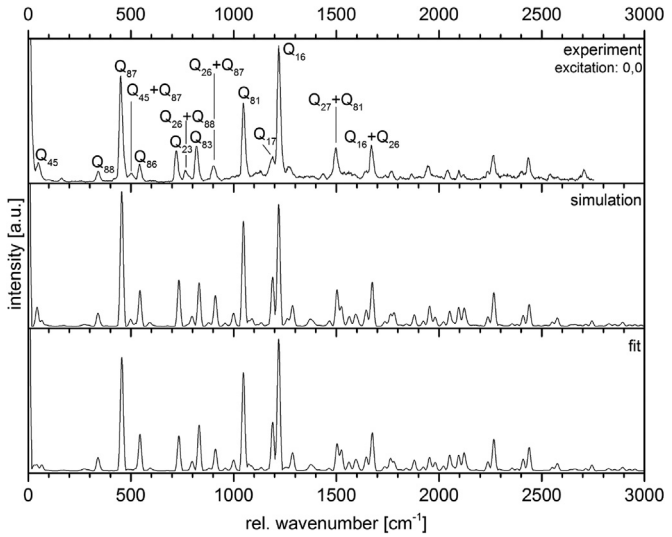

Fig. 6. Fluorescence emission spectrum of the 2-TN dimer upon excitation of the electronic origin at 35566.8 cm^{-1}.

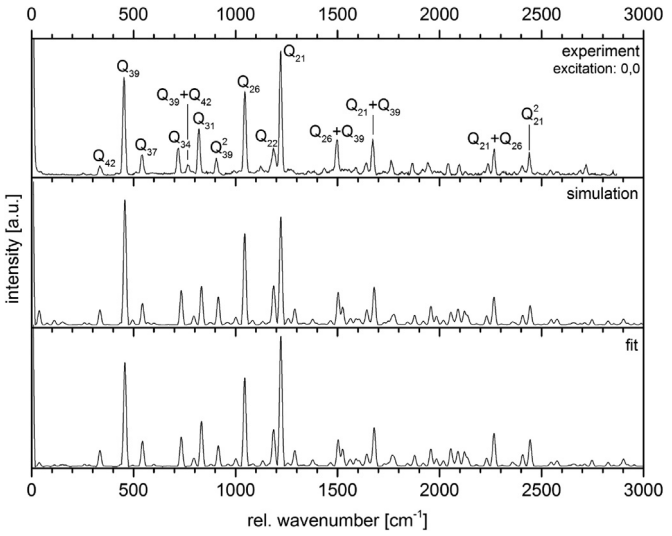

Fig. 7. Fluorescence emission spectrum of 2-TN-H_2 O upon excitation of the electronic origin at 35679.4 cm^{-1}.

monomer. We tentatively assigned the red-most band at 35566.8 cm^{-1} to the electronic origin of the 2-TN dimer and the energetically following bands blue-shifted by +11 and + 27 cm^{-1} to vibronic bands of the dimer. From comparison to the results of the normal mode analysis of the excited state of the dimer (cf. Table S6 of the online supporting material), both vibrations are of a" symmetry and can be assigned to the butterfly and the twisting motion of the two monomer moieties.

3.2.2. Single vibronic level fluorescence of $(2\text{-TN})_2$

The SVLF spectrum of the electronic origin of $(2\text{-TN})_2$ is shown in Fig. 6 along with a FC simulation using the *ab initio* optimized parameters and a FC fit, which was obtained as described in section 4. It shows strong FC activity in modes Q_{86} (b_u) and Q_{16} (a_g) and a rich FC spectrum up to an energy of 2000 cm^{-1}. Already the intensities from a FC simulation with the *ab initio* calculated geometries for ground and excited states show a very good agreement with the experimental intensities.

Additional SVLF spectra of the vibronic bands at 0,0 + 11 and 0,0 + 27 cm^{-1}, along with a Franck-Condon simulation and a FC fit are shown in the online supporting material (Figs. S1 and S2). A simultaneous fit of the intensities of all vibronic bands in the three emission spectra (given in Table S7 of the online supporting material) was performed in order to obtain the geometry changes of $(2\text{-TN})_2$ upon electronic excitation. The distortion along seven inter- and intramolecular normal modes Q serves as a basis for the geometry changes. Their values after fit are shown in Table S8 of the online supporting material.

3.2.3. Single vibronic level fluorescence of 2-TN-H_2O

The SVLF spectrum upon excitation of the electronic origin of 2-TN-H_2 O at 36442.9 cm^{-1} is shown in Fig. 7 along with a FC simulation using the *ab initio* optimized parameters and a FC fit, which was obtained as described in section 4. As for the 2-TN dimer, the agreement between the experimental and the fitted spectrum is good.

The distortion along ten inter- and intramolecular normal modes serve as a basis for the geometry changes. Their values after fit are shown in Table S11 of the online supporting material.

4. Discussion

In the FC fit of the emission band intensities, we adjust the excited state equilibrium geometry relative to the ground state geometry. The distortion of the excited state structure is performed by adding multiples ΔQ_i of the i-th column of the normal coordinate matrix **L** to the *ab initio* calculated Cartesian geometry. A subspace of the distortion parameters ΔQ is changed until best agreement between the computed and the observed vibronic intensities is reached.

4.1. The 2-TN dimer

We first discuss the electronic symmetries of the electronic states of 2-TN. As shown above, the S_1 state has B_u symmetry and is the one-photon allowed state, while the S_2 state is the (forbidden) A_g symmetric state. Other inversion symmetric dimers (benzonitrile dimer [3], benzoic acid dimer [6,7], pyrazine dimer [12]) behave differently and have the S_2-state as one-photon allowed B_u state. What is the difference between these dimers and $(2\text{-TN})_2$?

Most dimers investigated until now, are singly substituted benzene derivatives, which have their transition dipole moments along the short (b) inertial axes. The resulting two TDMs in these dimers are nearly parallel (H-aggregate) and the lower state is the A_g. The methyl group in 2-TN rotates the TDM away to a position nearly perpendicular to the bond attaching the methyl group to the benzene ring [32]. The resulting TDMs in the 2-TN dimer are nearly head-tail oriented (J-aggregates) and the lowest excited state of B_u symmetry is allowed, while the S_2 state (A_g) is forbidden. This behaviour has recently also been observed for the m-cyanophenol dimer by Balmer et al. [17] The two cases are compared in Fig. 8. The dipole-dipole interaction energy, V_{dd} which is shown as function of the angle θ between the dipole moments and the line connecting the two COMs is calculated from equation (4). The angle ϕ between the TDMs has been set to zero in this symmetric dimer, but one has to keep in mind, that upon isotopic substitution in one of the monomer moieties not only the Davydov splitting changes, but also the forbidden second component of the Davydov split bands becomes allowed. This has been shown for the benzonitrile dimer by Balmer et al. [4] and the benzoic acid dimer by Ottiger et al. [13]

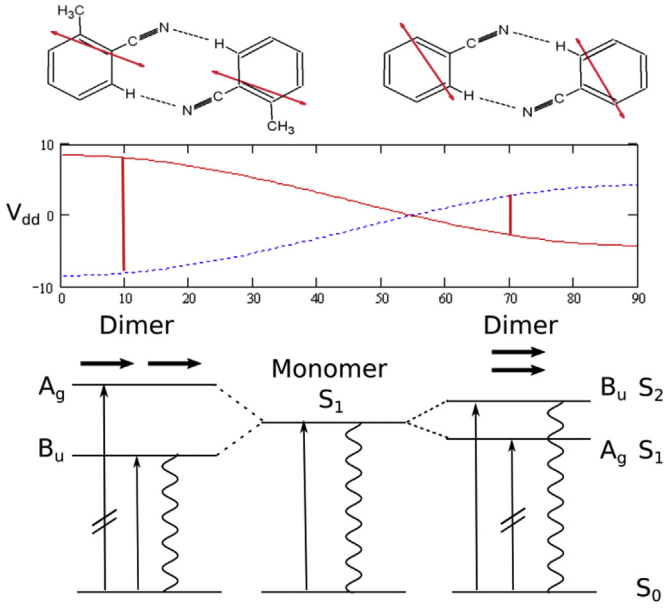

Fig. 8. Schematic drawing of the energetic ordering of the lowest two excited states in an inversion symmetric dimer. The left case refers to J-aggregates like for the 2-TN dimer, the right case to H-aggregates like for the benzonitrile dimer. The dipole-dipole interaction V_{dd} as function of the angle between the dipoles is shown, and the splitting for the $(2\text{-TN})_2$ and the $(\text{benzonitrile})_2$ are marked in the diagram.

Upon ^{13}C substitution in position 3 of one of the benzene rings in the benzonitrile dimer, Balmer et al. [4] showed, that the forbidden S_1 origin appears with nearly 50% of the intensity of the S_2, which was attributed to the symmetry reduction from C_{2h} to C_s. An interesting system to study would be the singly ^{13}C substituted benzonitrile dimer in position 1 of the benzene ring. Also for this isotopologue, the C_{2h} symmetry is broken, but since the substitution position lies on one of the main inertial axes of the monomer, the TDMs in both monomers would remain strictly parallel.

The Franck-Condon fit of the vibronic emission spectra of $(2\text{-TN})_2$ yields the changes of the bond parameters, shown in Fig. 9. Clearly, from the results of the FC fit the excitation is localized on one of the 2-TN chromophores. The bond length changes in one of the chromophores are considerably larger, than in the other, the changes being similar to the changes upon electronic excitation in the 2-TN monomer [31]. Not only the intramolecular bond length changes differ for both chromophores, but as well the intermolecular C≡N ··· H bond lengths are substantially different. One hydrogen bond gets considerably stronger, and the bond lengths decreases by 2.0 pm, while the other slightly increases by 0.4 pm.

This can be understood in the light of a natural population analysis (NPA), which has been performed for the monomer [31]. The interaction between the nitrogen atom lone pair (LP(N)) and

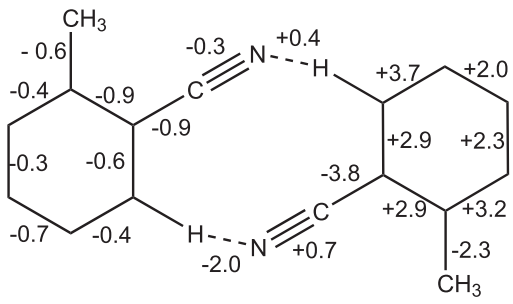

Fig. 9. Geometry changes of the 2-TN dimer from the FC fit.

the unoccupied Rydberg orbital at the neighboring C atom is strongly decreased upon electronic excitation. Therefore, the C≡N bond length increases. LP(N) interaction with the antibonding π orbital between the C atom of the nitrile group and the adjacent C atom also decreases. Thus, less electron density is shifted to the antibonding orbital upon electronic excitation, leading to a net increase of bond order and a resulting decrease of the C–C bond length. In turn, the higher LP(N) electron density in the excited state of 2-TN is responsible for the increase of bond order in the C≡N ··· H hydrogen bond, which manifests itself in the shortening by 2.0 pm (cf. Fig. 9). The second (H···N≡C) hydrogen bond increases by 0.4 pm upon electronic excitation.

In the SVLF spectra of the dimer, we observe emission from the C_s symmetric excited state. This is obvious from the fact, that all observed modes in the emission spectrum belong to the irreducible representation a' (corresponding to a_g and b_u vibrations in the C_{2h} point group). Thus, emission takes place from the C_s symmetric adiabatically lowest excited state with electronic A′ symmetry.

Additionally, we calculated the emission spectrum from the vibrationless origin of the C_{2h} symmetric S_2 state and compared it to the emission spectrum from the S_1 state and to the experimental spectrum. Fig. 10 shows the results of these calculations. Clearly the emission takes place from the S_1 state minimum, while the simulated emission from the vibrationless S_2 state is completely different from the experimental spectrum.

4.2. The 2-TN water cluster

For the 2-TN water cluster the situation is much clearer than for the 2-TN dimer. Since only one chromophore is present, there is no doubt about the site of excitation. The geometry changes upon electronic excitation are localized at the 2.TN chromophore, with the water molecule solvating the excited state after excitation.

Fig. 11 summarizes the geometry changes upon electronic excitation of the 2-TN-water cluster. The C≡N ··· H hydrogen bond length decreases, indicating the increase in bond strength upon electronic excitation of the chromophore. The second (H···O–H) hydrogen bond increases by 0.5 pm upon electronic excitation. The geometry changes in the chromophore are very similar to those of the uncomplexed monomer [31] and those of the excited moiety in the 2-TN dimer.

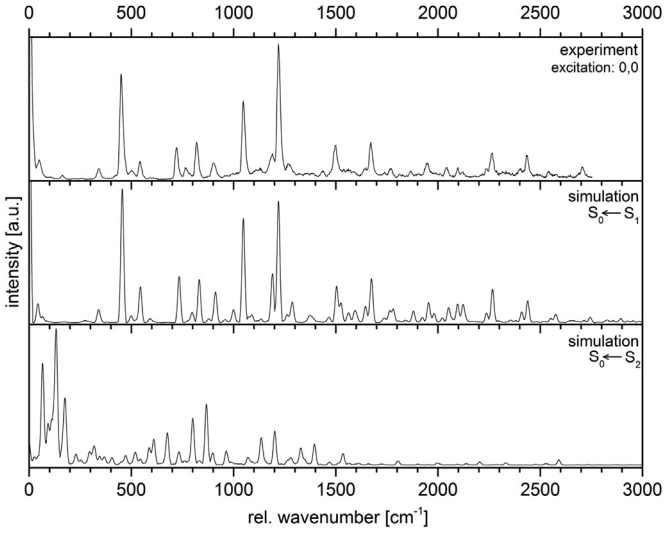

Fig. 10. Comparison of the experimental emission spectrum, obtained by pumping the electronic origin with the simulated $S_1 \leftarrow S_0$ and the $S_2 \leftarrow S_0$ spectra.

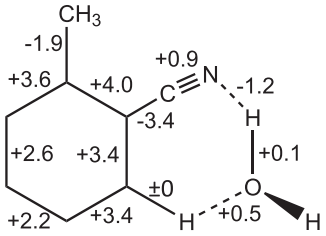

Fig. 11. Geometry changes of 2-TN-H_2O dimer from the FC fit.

5. Conclusions

The geometry changes upon electronic excitation in the 2-TN water cluster and in one of the two moieties of the 2-TN dimer are similar to those of the uncomplexed 2-TN monomer. Contrary to the cases of the benzonitrile dimer, benzoic acid dimer, 2-cyanophenol dimer, 3-cyanophenol dimer, azaindole dimer, pyridone dimer, which all form H-aggregates, the 2-TN dimer exhibits a J-aggregate structure. For all of the aforementioned dimers, the optically bright state is thus the S_2 with B_u symmetry, while the A_g symmetric S_1 state, exhibiting a double minimum potential is the bright state for the 2-TN dimer, cf. Fig. 8.

Even though the asymmetric excitation in one of the 2-TN moieties of the dimer suggests a localized excitation, the current experiment cannot make a distinction between localized and delocalized excitation. Emission spectra from the initially excited 2-TN moiety in the dimer or from the other moiety after excitation hopping will result in the same emission spectrum. Delocalized excitation in the context of the current experiments means that the semiclassical hopping time for excitation transfer between the monomers is shorter than the laser pulse duration of a few ns. This hopping time, which is the inverse of the resonance transfer rate can be estimated from the vibronic splitting:

$$\tau = 1/k_{AB} = \frac{h}{4|V_{AB}|} = \frac{1}{2\Delta_{vibron}c} \tag{8}$$

With the calculated value of the vibronic splitting of 6 cm^{-1} one obtains a hopping time of 2.7 ps. The value obtained here is shorter than for the H aggregates benzoic acid dimer (18 ps) [7] and benzonitrile dimer (8 ps) [4], but comparable to the J aggregate m-cyanophenol dimer (2.3 ps) [17]. However, one has to keep in mind that the dipole approximation used in the derivation of equation (8) is valid only if the distance of the dipoles is large compared to the lengths of the dipoles. This certainly is not the case for the dimers studied here, so the dipole approximation is a poor approximation in these cases and rate constants for resonant transfer rates must be considered with caution.

Furthermore, although not resolved in the current study, the electronic origin of the 2-TN dimer is split into three components due to the hindered internal rotation of the two equivalent methyl rotors [52]. These components arise from a splitting into an A_1, a G, an E_1 and an E_3 component with $A_1 - A_1$ (A-band), $G - G$ (G-band), and $(E_1 + E_3) - (E_1 + E_3)$ (E-band) selection rules. These torsional splittings cannot be resolved in the described experiments, but might be topic of a high resolution study on this system. However, the two E components of the origin band result from a geared and anti-geared motion of the two methyl rotors [52], which might be responsible for a symmetry breaking between the two monomer moieties in the dimer. Apart from their structural equality, this torsional motion would then introduce an in-equivalence of the two monomers. Such an in-equivalence has shown to be the reason for localization of the excitation in dimeric systems [13].

Acknowledgments

Computational support and infrastructure was provided by the "Center for Information and Media Technology" (ZIM) at the Heinrich-Heine-University Düsseldorf (Germany). The financial support of the Deutsche Forschungsgemeinschaft (SCHM 1043/12-3) is gratefully acknowledged. We thank Rainer Weinkauf, Samuel Leutwyler and Horst Köppel for helpful discussions.

Appendix A. Supplementary data

Supplementary data related to this article can be found at http://dx.doi.org/10.1016/j.molstruc.2017.04.092.

References

[1] T. Kobayashi, K. Honma, O. Kajimoto, S. Tsuchiya, J. Chem. Phys. 86 (1987) 1111–1117.
[2] M. Takayagani, I. Hanazaki, J. Opt. Soc. Am. B 7 (1990) 1898–1904.
[3] M. Schmitt, M. Böhm, C.R.S. Siegert, M. van Beek, W.L. Meerts, J. Mol. Struct. 795 (2006) 234–241.
[4] F.A. Balmer, P. Ottiger, S. Leutwyler, J. Phys. Chem. A 118 (2014) 11253–11261.
[5] K. Remmers, W.L. Meerts, I. Ozier, J. Chem. Phys. 112 (2000) 10890–10894.
[6] I. Kalkman, C. Vu, M. Schmitt, W.L. Meerts, ChemPhysChem 9 (2008) 1788–1797.
[7] P. Ottiger, S. Leutwyler, J. Chem. Phys. 137 (2012), 204303–1–204303–.
[8] S. Kopec, P. Ottiger, S. Leutwyler, H. Köppel, J. Chem. Phys. 142 (2015), 084308–1–084308–.
[9] N. Seurre, K.L. Barbu-Debus, F. Lahmani, A. Zehnacker-Rentien, J. Sepiol, Chem. Phys. 295 (2003) 21–33.
[10] K. Sakota, H. Sekiya, J. Phys. Chem. A 109 (1995) 2718–2721.
[11] A. Müller, F. Talbot, S. Leutwyler, J. Chem. Phys. 116 (2002) 2836–2847.
[12] A. Held, D.W. Pratt, J. Chem. Phys. 96 (1992) 4869–4876.
[13] P. Ottiger, H. Köppel, S. Leutwyler, Chem. Sci. 6 (2015) 6059–6068.
[14] S. Kopec, P. Ottiger, S. Leutwyler, H. Köppel, J. Chem. Phys. 137 (2012), 184312–1–084308–10.
[15] G. Scheibe, Angew. Chem. 50 (1937) 212–219.
[16] E.E. Jelley, Nature 139 (1937) 631–632.
[17] F.A. Balmer, S. Kopec, H. Köppel, S. Leutwyler, J. Phys. Chem. A 121 (2017) 73–87.
[18] J.A. Stearns, N.R. Pillsbury, K.O. Douglass, C.W. Mller, T.S. Zwier, D.F. Plusquellic, J. Chem. Phys. 129 (2008), 224305–1–224305–13.
[19] D.S. McClure, Can. J. Chem. 36 (1958) 59–71.
[20] A.S. Davydov, Sov. Phys. Usp. 7 (1964) 145.
[21] T. Förster, in: O. Sinanoglu (Ed.), Modern Quantum Chemistry, Academic Press, New York, 1965, pp. 93–137 ch. III B.
[22] M. Kasha, H.R. Rawls, M.A. El-Bayoumi, Pure Appl. Chem. 11 (1965) 371–392.
[23] J. Frenkel, Phys. Rev. 37 (1931) 1276.
[24] M. Fujii, M. Yamauchi, K. Takazawa, M. Ito, Spectrochim. Acta 50A (1994) 1421–1433.
[25] A.I. Jaman, S. Maiti, R.N. Nandi, J. Mol. Spec. 192 (2011) 148–151.
[26] A.I. Jaman, P.H. Kumar, P.R. Bangal, J. At. Mol. Opt. Phys. 2011 (2011), 480396–1–480396–8.
[27] H. Nakai, M. Kawai, J. Chem. Phys. 113 (2000) 2168–2174.
[28] C.H. Park, G.W. Lee, S.K. Lee, Bull. Korean Chem. Soc. 27 (2006) 881–885.
[29] C.H. Park, S.K. Lee, Bull. Korean Chem. Soc. 27 (2007) 1377–1380.
[30] K. Suzuki, S. Ishiuchi, M. Sakai, M. Fujii, J. Electr. Spect. Rel. Phen. 142 (2005) 215–221.
[31] F. Gmerek, B. Stuhlmann, L. Alvarez-Valtierra, D.W. Pratt, M. Schmitt, J. Chem. Phys. 144 (2016) 084304.
[32] J.A. Ruiz-Santoyo, J. Wilke, M. Wilke, J.T. Yi, D.W. Pratt, M. Schmitt, L. Alvarez-Valtierra, J. Chem. Phys. 144 (2016) 044303.
[33] R.M. Helm, H.P. Vogel, H.J. Neusser, V. Storm, D. Consalvo, H. Dreizler, Z. Naturforsch. 52 (1997) 655–664.
[34] S. Melandri, D. Consalvo, W. Caminati, P.G. Favero, J. Chem. Phys. 111 (1999) 3874–3879.
[35] M. Schmitt, U. Henrichs, H. Müller, K. Kleinermanns, J. Chem. Phys. 103 (1995) 9918–9928.
[36] W. Roth, C. Jacoby, A. Westphal, M. Schmitt, J. Phys. Chem. A 102 (1998) 3048–3059.
[37] R. Ahlrichs, M. Bär, M. Häser, H. Horn, C. Kölmel, Chem. Phys. Lett. 162 (1989) 165–169.
[38] J.T.H. Dunning, J. Chem. Phys. 90 (1989) 1007–1023.
[39] C. Hättig, F. Weigend, J. Chem. Phys. 113 (2000) 5154–5161.
[40] C. Hättig, A. Köhn, J. Chem. Phys. 117 (2002) 6939–6951.
[41] C. Hättig, J. Chem. Phys. 118 (2002) 7751–7761.
[42] P. Deglmann, F. Furche, R. Ahlrichs, Chem. Phys. Lett. 362 (2002) 511–518.
[43] TURBOMOLE V6.3 2012, a Development of University of Karlsruhe and Forschungszentrum Karlsruhe GmbH, 1989-2007, TURBOMOLE GmbH, since

2007 available from: http://www.turbomole.com.
[44] S.F. Boys, F. Bernardi, Mol. Phys. 19 (1970) 553–566.
[45] A.E. Reed, R.B. Weinstock, F. Weinhold, J. Chem. Phys. 83 (1985) 735–746.
[46] D. Spangenberg, P. Imhof, K. Kleinermanns, Phys. Chem. Chem. Phys. 5 (2003) 2505–2514.
[47] R. Brause, M. Schmitt, D. Spangenberg, K. Kleinermanns, Mol. Phys. 102 (2004) 1615–1623.
[48] E.V. Doktorov, I.A. Malkin, V.I. Man'ko, J. Mol. Spec. 56 (1975) 1–20.
[49] E.V. Doktorov, I.A. Malkin, V.I. Man'ko, J. Mol. Spec. 64 (1977) 302–326.
[50] W.H. Miller, J. Phys. Chem. 83 (1979) 960–963.
[51] J. Bicerano, H.F. Schaefer III, W.H. Miller, J. Am. Chem. Soc. 1105 (1983) 2550–2553.
[52] X.-Q. Tan, D.J. Clouthier, R.H. Judge, D.F. Plusquellic, J.L. Tomer, D. Pratt, J. Chem. Phys. 95 (1991) 7862–7871.